JOURNAL OF APPLIED PHYSICS 120, 055702 (2016)

Radial direct bandgap p-i-n GaNP microwire solar cells with enhanced short circuit current

Supanee Sukrittanon,[1] Ren Liu,[2] Michael C. Breeden,[3] Janet L. Pan,[2] K. L. Jungjohann,[4] Charles W. Tu,[1,2,a)] and Shadi A. Dayeh[1,2,a)]
[1]*Graduate Program of Materials Science and Engineering, University of California, San Diego, La Jolla, California 92037, USA*
[2]*Department of Electrical and Computer Engineering, University of California, San Diego, La Jolla, California 92037, USA*
[3]*Department of Nanoengineering, University of California, San Diego, La Jolla, California 92037, USA*
[4]*Center for Integrated Nanotechnologies, Sandia National Laboratories, Albuquerque, New Mexico 87185, USA*

(Received 17 April 2016; accepted 14 July 2016; published online 2 August 2016)

We report the demonstration of dilute nitride heterostructure core/shell microwire solar cells utilizing the combination of top-down reactive-ion etching to create the cores (GaP) and molecular beam epitaxy to create the shells (GaNP). Systematic studies of cell performance over a series of microwire lengths, array periods, and microwire sidewall morphologies examined by transmission electron microscopy were conducted to shed light on performance-limiting factors and to optimize the cell efficiency. We show by microscopy and correlated external quantum efficiency characterization that the open circuit voltage is degraded primarily due to the presence of defects at the GaP/GaNP interface and in the GaNP shells, and is not limited by surface recombination. Compared to thin film solar cells in the same growth run, the microwire solar cells exhibit greater short circuit current but poorer open circuit voltage due to greater light absorption and number of defects in the microwire structure, respectively. The comprehensive understanding presented in this work suggests that performance benefits of dilute nitride microwire solar cells can be achieved by further tuning of the epitaxial quality of the underlying materials. *Published by AIP Publishing.* [http://dx.doi.org/10.1063/1.4959821]

I. INTRODUCTION

Arrayed radial p-n junction microwires have garnered much attention recently as an additive or alternative to planar solar cells for enhancing solar conversion efficiency.[1–3] They offer potential for light-weight, portable, and flexible solar cells.[4–6] While Si-based radial-junction solar cells have been intensively researched in the past decade[7] and achieved recently an efficiency of ∼16.5% in array geometries,[8] it is known that multi-junction solar cells achieve higher efficiency than that of single-junction solar cells.[9] A simple exemplary configuration is a dual-junction solar cell that employs Si as the inner junction and 1.7 eV III–V semiconductor as the outer junction.[10–12] This configuration can theoretically deliver a maximum power conversion efficiency of 45% under AM 1.5 G.[13]

Dilute nitride GaNP is a promising candidate for the wide-bandgap junction in dual-junction solar cells because they exhibit a direct[14,15] and tunable[16,17] bandgap by incorporating a small amount of N (>0.4%) into GaP. This allows the bandgap of GaNP to be tuned to the optimal top-junction bandgap of 1.7 eV by incorporating only ∼4.5% of N, resulting in only ∼0.41% lattice mismatch with Si. Our previous study[18] demonstrated that ∼2.05 eV GaNP, nearly lattice-matched with Si, thin film solar cells on GaP substrate achieved a maximum efficiency of 7.3% in the absence of a window layer or an anti-reflection (AR) coating layer (7.9% with an AR coating). This GaNP solar cell's efficiency is higher than other wide-bandgap solar cells: 2.42%[19] for an indirect bandgap GaP (2.26 eV), 3.89%[20] for direct bandgap InGaP (2.12 eV), and 4.8%[21] for direct bandgap GaAsP (1.92 eV). Although there are studies focused on the integration of III–V onto Si wires,[22–25] to the best of our knowledge, no similar studies have fabricated and discussed GaNP microwire solar cells to date.

II. EXPERIMENT

In this work, we fabricated and demonstrated GaP/2.05 eV GaNP core/shell microwire solar cells on GaP (001) substrate. This GaNP shell layer is nearly lattice-matched with Si. All microwire samples are p-i-n solar cells that were fabricated by using a top-down dry etching technique to create p-GaP microwires that are free of planar defects,[26–28] followed by using a step-mediated growth approach by gas-source molecular beam epitaxy (MBE) to grow the surrounding i-GaNP and n-GaP shells to independently control their thickness and doping concentration. We performed systematic studies to evaluate the performance of GaNP microwire solar cells over a series of microwire lengths (L = 6 μm, 8 μm, 10 μm), array period (P = 4 μm, 6 μm, 8 μm), and morphology of microwire tips and sidewalls. The structural properties of the microwires were characterized by scanning electron microscopy (SEM) and transmission electron microscopy (TEM) to correlate microstructure details to the solar cell

[a)]Authors to whom correspondence should be addressed. Electronic addresses: ctu@ece.ucsd.edu and sdayeh@ece.ucsd.edu

performance. The solar cell performance was determined using current density–voltage (J–V) and external quantum efficiency (EQE) measurements.

Our p-i-n microwire structures are fabricated on highly doped p-type ($1.5 \times 10^{18}\,cm^{-3}$) GaP (001) substrate to form microwire cores with minimal series resistance to the back contact. The GaP core diameter was approximately 2 μm, which is comparable to the electron minority diffusion length of highly-doped p-GaP.[29] The next layer was a 500-nm-thick i-GaNP shell grown in MBE. GaNP was used to promote light absorption due to its direct bandgap, and an i-layer was employed to compensate for the short diffusion length in doped dilute nitride materials.[30,31] The final structure was a 100-nm-thick n-GaP ($4 \times 10^{18}\,cm^{-3}$) layer that acted as a standard emitter followed by a 15-nm-thick highly doped n^+-GaP ($8 \times 10^{18}\,cm^{-3}$) layer to reduce series resistances from the inner portions of the cell to the surrounding metal contacts.

The fabrication procedure of the microwires consists of reactive-ion-etching (RIE), wet etching, and shell growth in MBE. Photolithography was used to define the Ni dot array pattern, which was subsequently deposited with electron beam (e-beam) evaporation, and used as an etch mask. RIE etching was optimized to obtain vertical microwires in a 5 sccm of Cl_2 and 100 sccm of BCl_3 plasma under 200 W RIE power and 36.5 mTorr chamber pressure. This condition provided an etch rate of ~490 nm/min. After RIE was performed, the rough sidewalls of microwires were mitigated by a wet etch using $HCl{:}H_2O_2{:}H_2O = 1{:}1{:}1$ solution at room temperature. The wet etch process is crystal orientation-dependent, and is faster in ⟨110⟩ directions relative to ⟨100⟩ directions resulting in octagon-shaped structures with wide facets perpendicular to the ⟨110⟩ orientation.

After the wet etch process, the samples were loaded into a Varian Gen-II MBE system modified to handle gas sources to grow the i-GaNP and n-GaP shells in similar growth conditions to our previous reports.[18] After the shell growth, the microwires exhibited the formation of square sidewalls indicating anisotropic shell growth with faster growth rates in the ⟨100⟩ direction to eliminate the {110} facets formed during wet etching. The tips of the microwires featured square-like facets with various orientations that are influenced by energy minimization and the formation of twined structures as will be elaborated in the TEM analysis below. Based on the SEM observations of several shell growths, the growth rate of the shell corresponds to about one half of the growth rate on the planar layers.

To reduce nitrogen vacancy defects, we performed a post-growth rapid thermal annealing (RTA) step at 750 °C for 30 s in 95% N_2 and 5% H_2 forming gas ambient. We then fabricated multiple 1 mm × 1 mm solar cells per chip using photolithography and RIE processes to isolate between cells on the same chip. To achieve ohmic-like contact behavior with the top n-GaP, we deposited a Pd/Si front contact by e-beam evaporation and annealed the sample at 420 °C for 5 min in forming gas. The front contact is a picture frame that surrounds the microwires. To achieve ohmic-like back contact behavior with the p^+-GaP substrate, we evaporated Zn/Au in a filament/thermal evaporator and then annealed the contact in forming gas at 360 °C for 30 min.

III. RESULTS AND DISCUSSION

It is important for microwire cells to evaluate experimentally the geometrical effects on their performance, which we performed here for a fixed diameter of ~3 μm. Figures 1(a)–1(c) show 45° SEM images of arrays of microwires with a fixed length of 6 μm swept across array periods of 4 μm, 6 μm, and 8 μm. J–V characteristics of these samples, depicted in Figure 1(d) and listed in Table I, show an increase in the short circuit current density (J_{sc}) in microwires with tighter pitch (i.e., higher physical fill factor, PFF); the microwires with P = 4 μm exhibited a 16% higher J_{sc} compared to those with P = 8 μm. It should be noted that J_{sc} is generated by both the microwires and the underlying planar layer. These results are expected since microwires

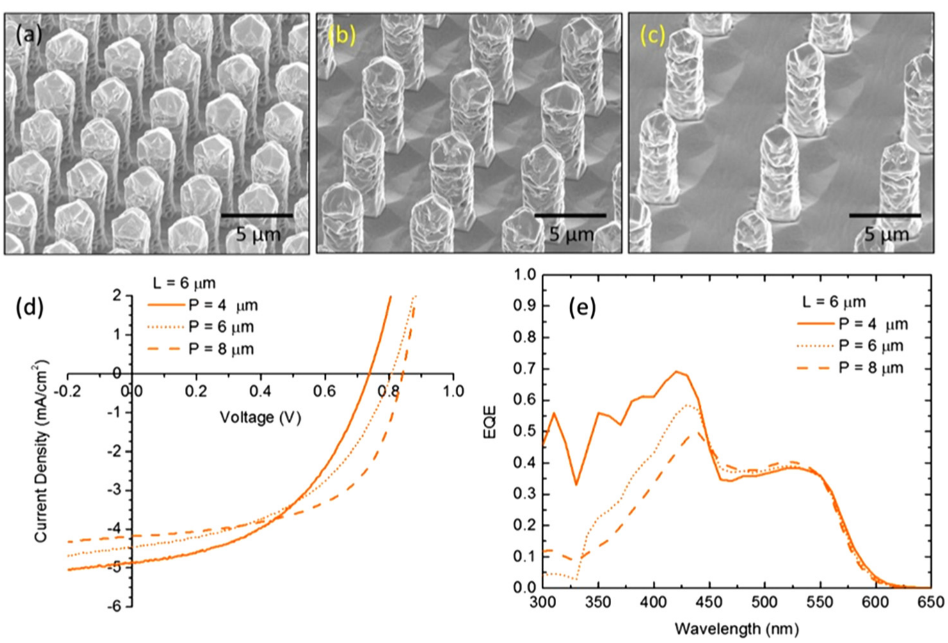

FIG. 1. (a)–(c) SEM images showing microwire arrays with L = 6 μm swept across different pitches of P = 4 μm, 6 μm, 8 μm, respectively. Their J–V characteristics and EQE are shown in (d) and (e), respectively.

TABLE I. Geometric and performance parameters for microwire solar cells with different lengths and array periods.

Length	P (μm)	J_{sc} (mA/cm^2)	V_{oc} (V)	FF	Efficiency (%)
6 μm	4	4.87	0.74	0.47	1.69
	6	4.46	0.81	0.47	1.70
	8	4.19	0.84	0.57	2.01
8 μm	4	5.48	0.71	0.50	1.96
	6	4.65	0.74	0.51	1.75
	8	4.13	0.82	0.55	1.86
10 μm	4	1.57	0.52	0.45	0.36
	6	4.85	0.78	0.52	1.95
	8	4.30	0.78	0.52	1.75

exhibit higher light absorption and more efficient carrier collection over thin films. In addition, it has been demonstrated theoretically and experimentally that the reflectance of the wires with facet tips is reduced when compared to planar surface or even wires with flat tips.[32] This increase of J_{sc} with higher PFF is accomplished with a reduction of V_{oc}.[24] This indicates that the gains of J_{sc} with tight pitch are outweighed by an increase in recombination currents. The increased recombination current in tight pitch can result from a larger recombination at (1) the microwire outmost non-passivated surface, (2) defective GaP/GaNP interface, and (3) defective GaNP shells. The fill factor (FF) decreases with higher PFF for the same reasons.

To delve further into the physics of operation of our microwire cells, we performed EQE measurements on the different pitch samples in the wavelength range of 300 nm to 650 nm. The EQE spectra, shown in Figure 1(e), show the absorption edges at ~615 nm for all samples indicating that the GaNP shells possess a bandgap of ~2.05 eV. All microwires exhibited two EQE peaks.[18] The short wavelength peak (~350 nm to ~450 nm) stems primarily from the GaP layer, while the long wavelength peak (~450 nm to ~615 nm) stems primarily from the GaNP layer. As the PFF of the microwires increases, we observe that short wavelength EQE increases, yet there is no significant change in long wavelength EQE. This implies that the increase in short wavelength EQE is the main contributor in the enhancement of J_{sc}. This could result from better short-wavelength absorption in the microwires compared to the underlying planar layers. It should be noted that short wavelength light is primarily absorbed in the highly-doped emitter layer. The thin film emitter (~230 nm), due to MBE growth, is two times thicker than the microwire emitter (~115 nm). This thin film emitter, which is thicker than the hole-minority diffusion length (~190 nm[19]), results in high recombination and degraded short-wavelength EQE. As a result, the thinner emitter layer of the microwires provides significant gains in short wavelength EQE compared to the underlying thin films. Higher short-wavelength EQE at higher PFF also implies that surface recombination, which is primarily related to short wavelength performance, do not exhibit a major negative impact on microwire J_{sc}. This observation suggests that surface recombination is not a major factor in the V_{oc} degradation discussed earlier.

In order to understand the effect of microwire length on performance, we also fabricated and studied longer microwires. Microwire pattern and period were kept the same as in Figure 1 and only length was varied as L = 8 μm and L = 10 μm. The resulting J–V characteristics and EQE spectra are depicted in Figure 2. For L = 8 μm, J–V characteristics show that J_{sc} increases and V_{oc} decreases with microwire array density, and the EQE results show that J_{sc} is sensitive to short wavelengths. Both observations are in line with the

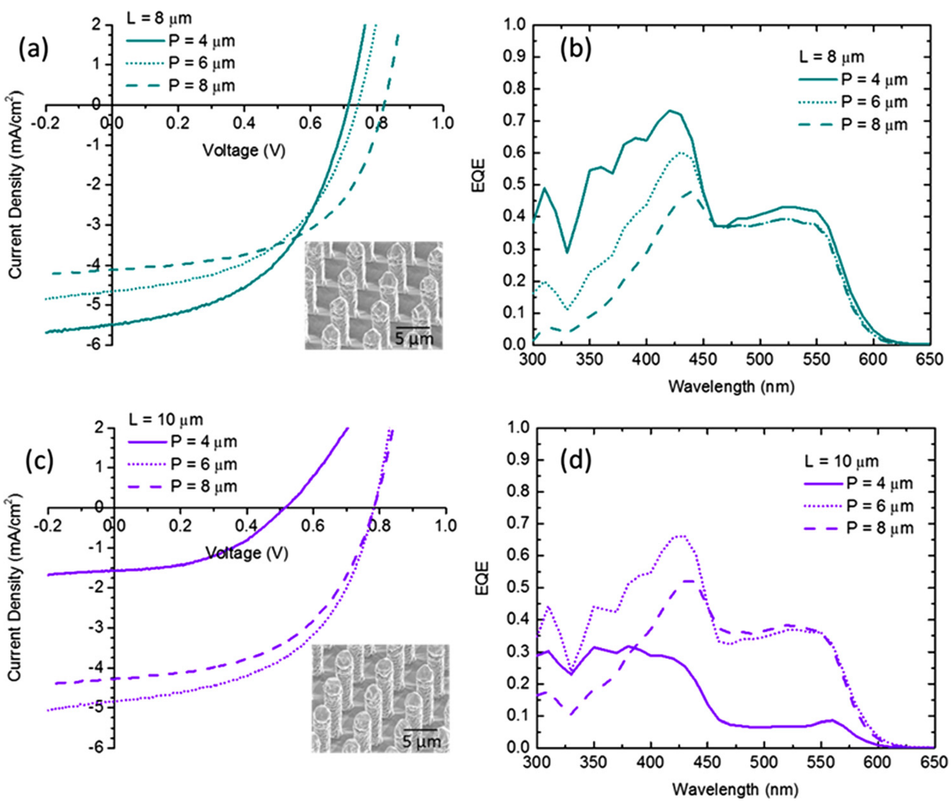

FIG. 2. J–V characteristics and EQE of microwire solar cells with different pitch for (a), (b) 8-μm-long microwire solar cells, and (c) and (d) 10-μm-long microwire solar cells.

L = 6 μm sample. This trend continues for L = 10 μm with the exception of the P = 4 μm sample. The P = 4 μm sample exhibited much lower J_{sc} and V_{oc} compared to other microwires in this study which we attribute to MBE shadow effects in the directional MBE growth, which is exacerbated by the length of the microwire. Excluding this result, we conclude that for a fixed period, J_{sc} increases as microwire length increases.[23] This effect is more pronounced in higher PFF, which is as expected.

To investigate the crystal quality of the microwire solar cell, TEM analysis was performed along [110] zone axis on the 6-μm-long microwire with P = 6 μm, as an example. From TEM images shown in Figure 3, we observed that the microwire possesses a large linear density of $\sim 5 \times 10^4$/cm of stacking faults in the GaNP shell and a misfit edge linear dislocation density of 2.4×10^5/cm at the GaP/GaNP interface along its length. These defects are clearly apparent in two g-vector orientations (Figures 3(c) and 3(d), g = [$\bar{1}1\bar{1}$]; Figs. 5(e) and 5(f), g = [$11\bar{1}$]) and under both bright-field and dark-field conditions. We believe that these defects are the main cause of V_{oc} degradation in the microwire solar cells with high PFF. The occurrence of interface defects in the microwire is greater than what is seen in our previous work of GaP/GaNP thin films.[18] This implies that the number of defects at the GaP/GaNP interface of the microwire is not only a result from GaP/GaNP lattice mismatch, but a result from the surface roughness of the core prior to the shell growth. While wet etch smoothening can help to mitigate the issue, we were unable to completely eliminate the introduction of interface defects resulting from the sidewall roughness in our experiment. To decrease the number of defects both at GaP/GaNP interface and in the shell, we repeated our previous experiment for L = 6 μm and P = 6 μm with the only difference being that we performed a slower wet etch to further smoothen the rough core sidewalls caused by RIE. After shell growth, the resultant SEM image, Figure 4(a), shows smoother shell sidewalls (and also less defective from TEM analysis discussed next). Despite some slight roughness, henceforth, these microwires are referred to as smooth microwires. To compare solar cell performance with different sidewall morphologies, J–V characteristics were performed under dark and AM 1.5 G conditions on this smooth microwire sample and compared against the measurements performed on the original (rough) microwire sample, which feature the same length and array period.

Maximum ideality factors calculated from the slope of the semi-log dark J–V curve, shown in Figure 4(b), are 3.5 and 4.8 for the smooth microwires and rough microwires, respectively. This higher ideality factor in the rough microwires indicates that the rough microwires suffer higher recombination rates,[33] which results in greater recombination current and consequently degrades the V_{oc} performance. It is noted that both microwires possess the ideality factor >2. This results from their edge dislocations and interface defects, which are shown in Figures 3 and 5 for the rough microwires and the smooth microwires, respectively.

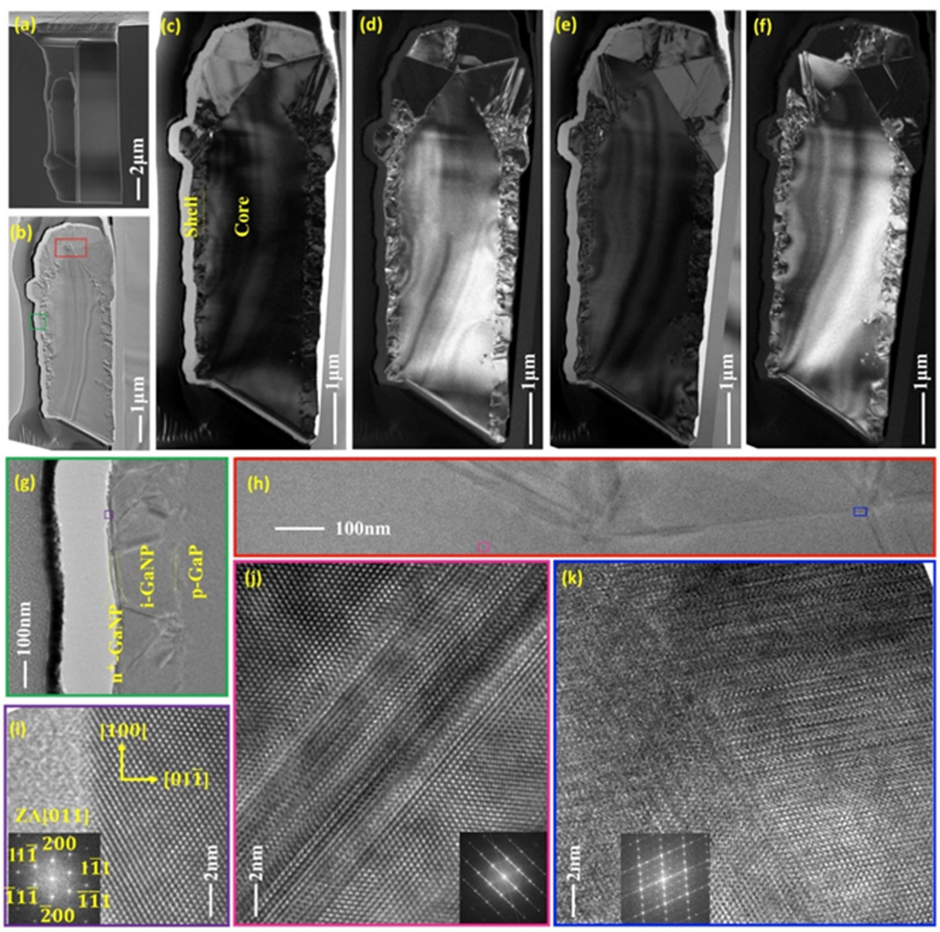

FIG. 3. (a) Overview SEM image of the sample on TEM grid after FIB cut and thinning. (b) Overview TEM image of the studied microwire. (c) and (d) Bright-field and dark-field images of the microwire along a [011] zone axis with a [$\bar{1}1\bar{1}$] g vector. (e) and (f) The bright-field and dark-field TEM images along [011] zone axis with the g vector of [$11\bar{1}$]. (g) and (h) The high magnification TEM image at the edge and center of microwire tip in the regions highlighted by green and red squares in (b), respectively. (i) HRTEM image of the edge of the microwire in the highlighted yellow square in (g). (j) and (k) The HRTEM images at the center of microwire tip in the regions highlighted by pink and blue squares in (h). Insets in (i), (j), and (k) are the correspondent FFT patterns from the HRTEM images validating micro-twinned and defective shells.

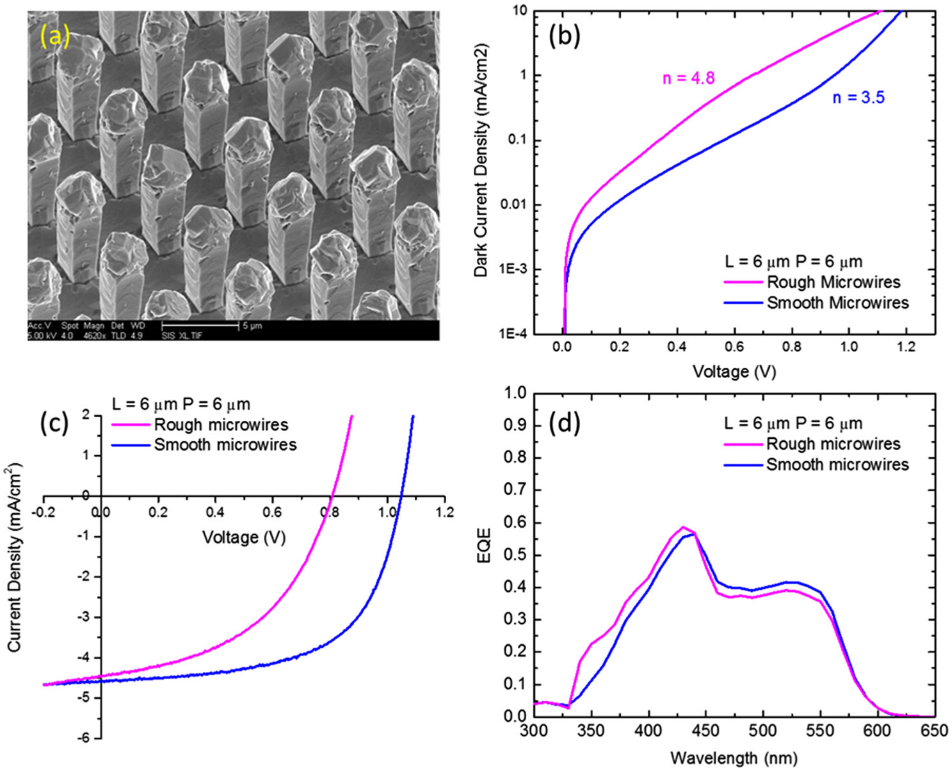

FIG. 4. (a) SEM image with much smoother microwires sidewalls. J–V characteristics of solar cells with rough and smooth microwire sidewalls under dark (b) and light (c). (d) EQE of the two samples.

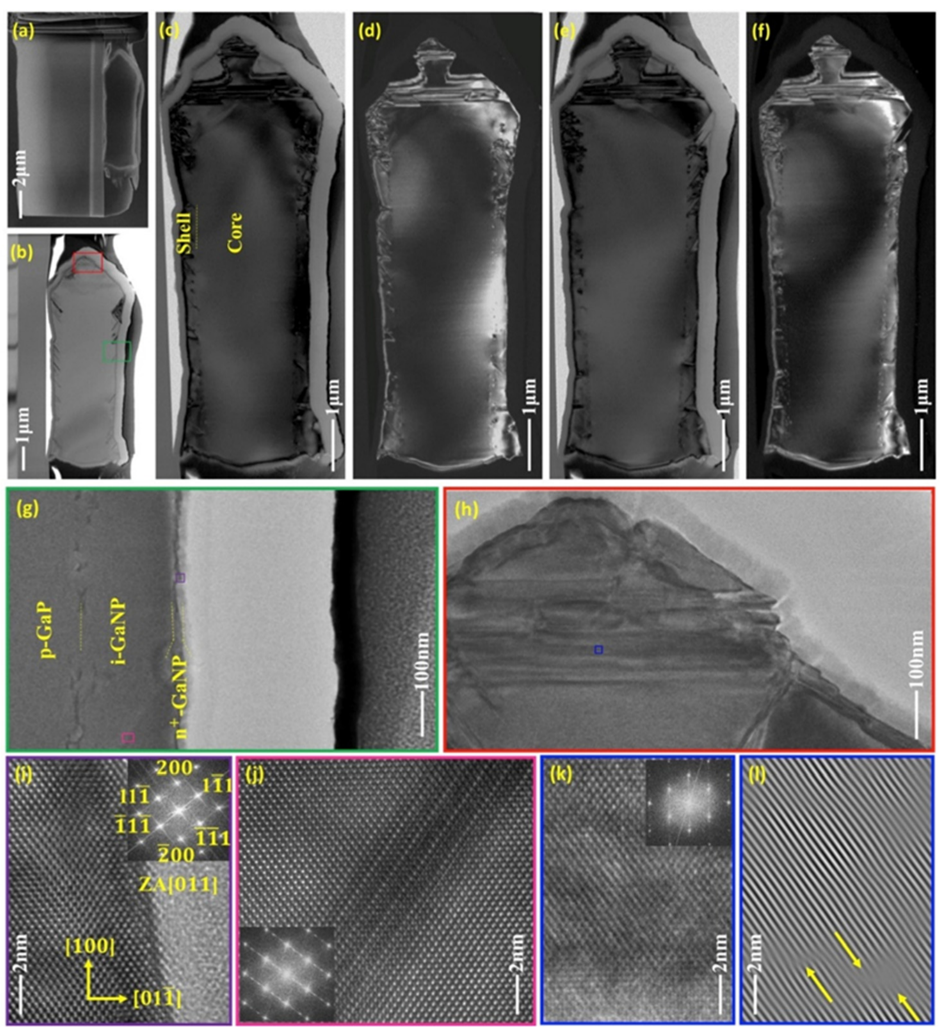

FIG. 5. (a) Overview SEM image of the sample on TEM grid after FIB cut and thinning. (b) Overview TEM image of the studied microwire. (c) and (d) Bright-field and dark-field images of the microwire along a [011] zone axis with a $[\bar{1}1\bar{1}]$ g vector. (e) and (f) The bright-field and dark-field TEM images along [011] zone axis with the g vector of $[11\bar{1}]$. (g) and (h) The high magnification TEM image at the edge and center of microwire tip in the regions highlighted by green and red squares in (b), respectively. (i)–(j) HRTEM images at the surface of the microwire and in the shell, respectively, as highlighted in purple and pink squares in (g). (k) The HRTEM image at the center of microwire tip in the regions highlighted by a blue square in (h). Insets in (i), (j), and (k) are the correspondent FFT patterns from the HRTEM images. (l) Inverse FFT image from inset in (k) showing several extra planes indicative of dislocations in the imaged region.

According to the J–V curves under light condition, the sample with smooth sidewalls exhibit significant improvement in V_{oc} performance over the sample with rough sidewalls, as shown in Figure 4(c). This is in line with the results from the dark current. This is a direct evidence to confirm that defects in the shell layer and interfacial defects have a major impact on the V_{oc} performance in the microwire solar cells. FF is also improved with the smooth microwires as expected due to their lower ideality-factors. However, we note that sidewall morphology has no significant impact on J_{sc}, as no change of J_{sc} was observed. The EQE results, as depicted in Figure 4(d), also showed negligible change as a result of sidewall smoothening. It should be noted that rough sidewalls do provide the benefit of better light absorption due to good coupling of incident light,[23] but this benefit is offset by poorer minority carrier collection in these microwires resulting in no significant change in J_{sc} performance between rough and smooth samples.

To confirm the lower occurrence of defects in the microwires with smooth sidewalls, TEM along [110] zone axis was performed in the methodology previously described in Figure 3. Figure 5 shows that the smooth microwire possesses much fewer stacking faults in the GaNP shell at a linear density of $\sim 2.4 \times 10^4$/cm and relatively similar linear density of edge dislocations of $\sim 2.1 \times 10^5$/cm at the GaP/GaNP interface along the microwire length when compared to the microwires with rough sidewalls. The tip of these microwires, however, continues to suffer from stacking fault defects and some rotational twins, less than that of rough microwires. Overall, there is an obvious reduction of defects in the shell along the length of the microwire which we speculate have helped in achieving longer hole minority carrier diffusion lengths in the shell and a lower recombination current. This result is in line with the aforementioned J–V characteristics. It should be noted that these defects are still greater than the defects observed in thin film solar cell, suggesting significant challenges in the preparation of epi-ready surfaces on the microwires when compared to planar surfaces.[17]

To exploit additional strategies in optimizing light absorption and microwire cell performance, we also investigated the impact of AR coatings. A $TiO_2/Si_3N_4/SiO_2$ (33 nm/52 nm/88 nm) triple-layer AR coating was deposited on the smooth microwire sample. This AR coating was calculated and measured to have low reflectivity (<5%) across 400–700 nm wavelengths. The AR coating provided an appreciable improvement in J_{sc} and a slight improvement in V_{oc}. The EQE measurement revealed that the increased J_{sc} resulted from improved light response for short and medium wavelengths but not for long wavelengths near the band edge. From this, we infer that the long-wavelength EQE is not limited by the reflection of light but is, instead, limited by the i-GaNP thickness. It should be noted that the long-wavelength EQE (500 nm to 615 nm) corresponds to the absorption and carrier collection only in i-GaNP. GaP, which has larger bandgap, cannot absorb those long-wavelength photons. Thus far, our best microwire sample achieves an efficiency of 3.2% with $J_{sc} = 5.01$ mA/cm^2, $V_{oc} = 1.07$ V, and FF = 0.60.

TABLE II. Performance metrics of microwire solar cells (L = 6 μm and P = 6 μm) with different sidewall morphologies, after AR coating and also the parameters from the thin film solar cell in the same growth run.

	J_{sc} (mA/cm^2)	V_{oc} (V)	FF	Efficiency (%)	Ideality factor
Rough microwires	4.46	0.81	0.47	1.7	4.8
Smooth microwires	4.57	1.05	0.60	2.9	3.5
Smooth microwires with AR	5.01	1.07	0.60	3.2	…
Thin film	4.17	1.36	0.77	4.4	1.8

IV. CONCLUSIONS

In conclusion, we have successfully fabricated GaP/GaNP core/shell microwires utilizing top-down dry etching to create the microwire cores and MBE to create the shells. The following are some highlights of our results. First, for a fixed length, J_{sc} increases with increasing PFF. This improvement in J_{sc} stems primarily from better response in short-wavelength light. Second, for a fixed array period, J_{sc} increases as microwire length increases. Third, the degradation of V_{oc} in our microwire sample is caused primarily by defects at the GaP/GaNP interface and in the shells. Surface recombination does not show a substantial negative impact on microwire performance in our experiment. Finally, our best efficiency from microwire solar cell is 3.2% with smooth sidewalls and AR coating. Compared to the thin film solar cell in the same growth run, the parameters for which are listed in Table II, our best microwire solar cell exhibits greater J_{sc} but poorer V_{oc}. This results from a greater number of defects in the microwire structure. For future work, optimization of core fabrication and shell growth process must be studied with the goal of minimizing defects. We believe that mitigating defects will enable GaNP microwire solar cells to surpass the performance of thin film GaNP solar cells.

ACKNOWLEDGMENTS

This work was supported by the National Science Foundation under Grant Nos. DMR-1106369, DMR-1503595, and ECCS-1351980. The TEM work was performed at the Center for Integrated Nanotechnologies (CINT), U.S. Department of Energy, Office of Basic Energy Sciences User Facility at Los Alamos National Laboratory (Contract No. DE-AC52-06NA25396) and Sandia National Laboratories (Contract No. DE-AC04-94AL85000).

[1] J. Yoo, B. M. Nguyen, I. H. Campbell, S. A. Dayeh, P. Schuele, D. Evans, and S. Tom Picraux, ACS Nano **9**(5), 5154 (2015).

[2] G. Mariani, Z. Zhou, A. Scofield, and D. L. Huffaker, Nano Lett. **13**(4), 1632 (2013).

[3] B. M. Kayes, H. A. Atwater, and N. S. Lewis, J. Appl. Phys. **97**(11), 114302 (2005).

[4] K. T. Park, Z. Guo, H. D. Um, J. Y. Jung, J. M. Yang, S. K. Lim, Y. S. Kim, and J. H. Lee, Opt. Express **19**(S1), A41 (2011).

[5] K. T. Park, H. J. Kim, M. J. Park, J. H. Jeong, J. Lee, D. G. Choi, J. H. Lee, and J. H. Choi, Sci. Rep. **5**, 12093 (2015).

[6] N. Han, Z. X. Yang, F. Wang, G. Dong, S. P. Yip, X. Liang, T. F. Hung, Y. Chen, and J. C. Ho, ACS Appl. Mater. Interfaces **7**(36), 20454 (2015).

[7] M. Gharghi, E. Fathi, B. Kante, S. Sivoththaman, and X. Zhang, Nano Lett. **12**(12), 6278 (2012).

[8]H. D. Um, I. Hwang, N. Kim, Y. J. Yu, M. Wober, K. H. Kim, and K. Seo, Adv. Mater. Interfaces **2**(16), 1500347 (2015).
[9]M. A. Green, K. Emery, Y. Hishikawa, W. Warta, and E. D. Dunlop, Prog. Photovoltaics: Res. Appl. **23**(7), 805 (2015).
[10]N. Jain and K. H. Mantu, Energy Harvesting Syst. **1**(3), 121 (2014).
[11]S. R. Kurtz, P. Faine, and J. M. Olson, J. Appl. Phys. **68**(4), 1890 (1990).
[12]J. F. Geisz and D. J. Friedman, Semicond. Sci. Technol. **17**(8), 769 (2002).
[13]T. J. Grassman, J. A. Carlin, C. Ratcliff, D. J. Chmielewski, and S. A. Ringel, in Proceedings of the IEEE 39th Photovoltaic Specialists Conference (PVSC) (2013), p. 0149.
[14]H. P. Xin, C. W. Tu, Y. Zhang, and A. Mascarenhas, Appl. Phys. Lett. **76**(10), 1267 (2000).
[15]I. A. Buyanova, G. Pozina, J. P. Bergman, W. M. Chen, H. P. Xin, and C. W. Tu, Appl. Phys. Lett. **81**(1), 52 (2002).
[16]W. Shan, W. Walukiewicz, K. M. Yu, J. Wu, J. W. Ager, E. E. Haller, H. P. Xin, and C. W. Tu, Appl. Phys. Lett. **76**(22), 3251 (2000).
[17]W. G. Bi and C. W. Tu, Appl. Phys. Lett. **69**(24), 3710 (1996).
[18]S. Sukrittanon, R. Liu, Y. G. Ro, J. L. Pan, K. L. Jungjohann, C. W. Tu, and S. A. Dayeh, Appl. Phys. Lett. **107**(15), 153901 (2015).
[19]L. Xuesong, S. Huang, M. B. Diaz, N. Kotulak, H. Ruiying, R. Opila, and A. Barnett, IEEE J. Photovoltaics **2**(2), 214 (2012).
[20]S. Tomasulo, K. Nay Yaung, J. Faucher, M. Vaisman, and M. L. Lee, Appl. Phys. Lett. **104**(17), 173903 (2014).
[21]S. Tomasulo, K. Nay Yaung, J. Simon, and M. L. Lee, Appl. Phys. Lett. **101**(3), 033911 (2012).
[22]A. C. Tamboli, M. Malhotra, G. M. Kimball, D. B. Turner-Evans, and H. A. Atwater, Appl. Phys. Lett. **97**(22), 221914 (2010).
[23]D. B. Turner-Evans, C. T. Chen, H. Emmer, W. E. McMahon, and H. A. Atwater, J. Appl. Phys. **114**(1), 014501 (2013).
[24]N. C. Strandwitz, D. B. Turner-Evans, A. C. Tamboli, C. T. Chen, H. A. Atwater, and N. S. Lewis, Adv. Energy Mater. **2**(9), 1109 (2012).
[25]C. T. Chen, D. B. Turner-Evans, H. Emmer, S. Aloni, and H. A. Atwater, in Proceedings of the IEEE 39th Photovoltaic Specialists Conference (PVSC) (2013).
[26]S. Sukrittanon, Y. J. Kuang, A. Dobrovolsky, W.-M. Kang, J.-S. Jang, B.-J. Kim, W. M. Chen, I. A. Buyanova, and C. W. Tu, Appl. Phys. Lett. **105**(7), 072107 (2014).
[27]P. Caroff, K. A. Dick, J. Johansson, M. E. Messing, K. Deppert, and L. Samuelson, Nat. Nanotechnol. **4**(1), 50 (2009).
[28]T. Burgess, S. Breuer, P. Caroff, J. Wong-Leung, Q. Gao, H. Hoe Tan, and C. Jagadish, ACS Nano **7**(9), 8105 (2013).
[29]M. L. Young and D. R. Wight, J. Phys. D: Appl. Phys. **7**(13), 1824 (1974).
[30]M. Da Silva, S. Almosni, C. Cornet, A. Létoublon, C. Levallois, P. Rale, L. Lombez, J. F. Guillemoles, and O. Durand, Proc. SPIE **9358**, 93580H (2015).
[31]S. Kurtz, A. Ptak, S. Johnston, C. Kramer, M. Young, D. Friedman, J. Geisz, W. McMahon, A. Kibbler, J. Olson, R. Crandall, and H. Branz, *Understanding the Potential and Limitations of Dilute Nitride Alloys for Solar Cells* (NREL, 2005).
[32]G. Anjia, H. Yijie, H. Shu, T. Sarmiento, E. Pickett, L. Dong, L. Shuang, A. Lin, S. Thombare, Y. Zongfu, F. Shanhui, P. McIntyre, Y. Cui, and J. Harris, in Proceedings of the 35th IEEE Photovoltaic Specialists Conference (PVSC) (2010).
[33]J. Nelson, *The Physics of Solar Cells*, 1st ed. (Imperial College Press, 2003).